Experimental Characterization of Entanglement Dynamics in Noisy Channels

Jin-Shi Xu, Chuan-Feng Li,* Xiao-Ye Xu, Cheng-Hao Shi, Xu-Bo Zou,† and Guang-Can Guo

Key Laboratory of Quantum Information, University of Science and Technology of China, CAS, Hefei, 230026, People's Republic of China

(Received 21 May 2009; published 9 December 2009; publisher error corrected 20 May 2010)

We experimentally characterize the bipartite entanglement under one-sided open system dynamics and verify the recently formulated entanglement factorization law [Nature Phys. **4**, 99 (2008)]. The one-sided open system dynamics is realized by implementing a phase damping and an amplitude decay channel, respectively, acting on one of the qubits, by an all-optical setup. Our results greatly simplify the characterization of entanglement dynamics and will play an important role in the construction of complex quantum networks.

DOI: 10.1103/PhysRevLett.103.240502 PACS numbers: 03.67.Mn, 03.65.Ud, 03.65.Yz, 05.40.Ca

Characterizing the dynamics of entanglement in noisy channels is an important task for entanglement-based quantum information processing [1]. Usually, the tomography process [2] which requires measurement on a complete set of observable quantities is used to reconstruct the final density matrix ρ and the entanglement is always nonlinearly dependent on it [3]. Therefore, the knowledge of entanglement dynamics can only be deduced from the time evolution of the state in this method [4–7]. Such a state-dependent process can be illustrated clearly from the commonly used concurrence quantifying entanglement between two particles [8], which is given by

$$C = \max\{0, \Gamma\}, \tag{1}$$

where $\Gamma = \sqrt{\lambda_1} - \sqrt{\lambda_2} - \sqrt{\lambda_3} - \sqrt{\lambda_4}$ with λ_i denoting the eigenvalues in decreasing order of the matrix $\rho(\sigma_y \otimes \sigma_y)\rho^*(\sigma_y \otimes \sigma_y)$. σ_y is the second Pauli matrix and ρ^* is the complex conjugate of ρ in the canonical basis $\{|00\rangle, |01\rangle, |10\rangle, |11\rangle\}$. As a result, the concurrence depends on the exact form of ρ.

However, Konrad *et al.* [9] present a general factorization law on entanglement dynamics of biparticle systems under the action of an arbitrary channel \$ on one of the components. The main result they get is the formulation

$$C[(\mathbb{1} \otimes \$)|\chi\rangle\langle\chi|] = C[(\mathbb{1} \otimes \$)|\phi^+\rangle\langle\phi^+|]C(|\chi\rangle), \tag{2}$$

where $|\chi\rangle$ is the initial input pure state and $|\phi^+\rangle$ is the maximally entangled state. For simplicity, we use C_{LP} and C_{RP} to represent the left and right terms of the equality, respectively. It is clearly shown that the entanglement dynamics of a pure state in the one-sided noisy channel only relates to the dynamics of the maximally entangled state in the same channel with a factor of initial concurrence.

Because of the convexity property of concurrence [8], this factorization law can be generalized to the mixed initial state ρ_0 [9]

$$C[(\mathbb{1} \otimes \$)\rho_0] \leq C[(\mathbb{1} \otimes \$)|\phi^+\rangle\langle\phi^+|]C(\rho_0). \tag{3}$$

We also use C_{LM} (C_{RM}) to represent the left (right) term of this inequality. It is shown that C_{RM} gives the upper bound of the evolved entanglement. If the initial mixed state ρ_0 is obtained as the result of a one-sided channel \$′ acting on a pure state $|\chi\rangle$, i.e., $\rho_0 = (\mathbb{1} \otimes \$')|\chi\rangle\langle\chi|$, and the concurrence dynamics of $|\phi^+\rangle$ under all the channels ($\mathbb{1} \otimes \$'$, $\mathbb{1} \otimes \$$, and the concatenation of them) follows the exponential decay form, then the equality holds in (3) [9].

The factorization law has been verified in an amplitude decay channel which is simulated by a modified Sagnac interferometer [10]. In their experiment, the concurrence of the evolved maximally entangled state ($C[(\mathbb{1} \otimes \$)|\phi^+\rangle\langle\phi^+|]$) is obtained from the experimental form of the single channel \$ [10]. Here, we experimentally verify the factorization law of two-photon entanglement dynamics with one of the photons passing through different noisy channels, i.e., the phase damping channel and the amplitude decay channel. We measure all the quantities in equality (2) and inequality (3), and then compare the left terms and the right terms to directly verify the validity of characterizing the entanglement dynamics in noisy channels with the maximally entangled state.

Our experimental setup is shown in Fig. 1. Ultraviolet (UV) pulses with wavelength centered at 390 nm are frequency doubled from a Ti:sapphire laser with a pulse width of 130 fs and a repetition rate of 76 MHz. These pulses pump two adjacent type I beta-barium-borate (BBO) crystals with their optical axes aligned in perpendicular planes to generate entangled photon pairs [11]. The polarization of the pump light is set by the half wave plate HWP0 which can be used to prepare different pure state $|\chi\rangle = \alpha|HH\rangle_{a,b} + \beta|VV\rangle_{a,b}$. H (V) represents the horizontal (vertical) polarization and the subscript a (b) denotes the path of the photon. α and β are the relative amplitudes which are set to be real for simplicity with $\alpha^2 + \beta^2 = 1$. Quartz plates (CP) in both emitted modes a and b are used to compensate the temporal difference between horizontal and vertical polarization components in these two nonlinear crystals [12].

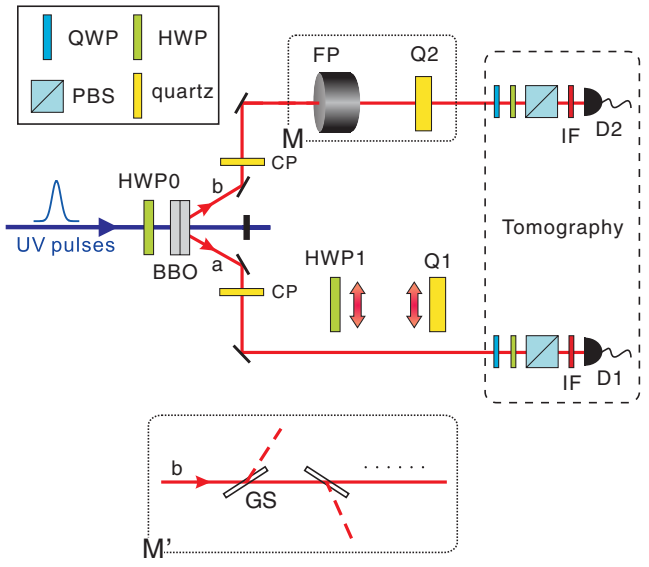

FIG. 1 (color online). The experimental setup to investigate the entanglement dynamics in different noisy channels. Entangled polarization photon pairs generated from the adjacent nonlinear crystals (BBO) emit into modes a and b. Quartz plates (CP) are used to compensate the temporal difference between different polarization components. The half wave plate (HWP0) is used to change the polarization of the pump light. A half wave plate (HWP1) and quartz plates ($Q1$) are inserted into mode a depending on different cases. The dotted panes M and M' represent the noisy channels. The Fabry-Perot (FP) cavity followed by quartz plates ($Q2$) in M simulates the phase damping channel, while the set of glass slabs (GS) tilted near Brewster's angle in M' represents the amplitude decay channel (the dashed lines represent the paths of reflected photons). Quarter wave plates (QWP), half wave plates (HWP), and polarization beam splitters (PBS) in both arms are used to set the detecting polarization bases for the state reconstruction. Both photons are finally detected by silicon avalanche photodiodes ($D1$ and $D2$) equipped with 3 nm interference filters (IF) to give coincident counts.

A Fabry-Perot (FP) cavity followed by quartz plates $Q2$ in the dotted pane M is used to simulate the phase damping channel. It is a kind of non-Markovian environment and has been used in our previous experiment [13]. When the photon in mode b with frequency ω_b passes through $Q2$ with thickness L, the relative phase between H and V polarizations is calculated by $\delta_b = L\Delta n\omega_b/c$, where c is the velocity of the photon in the vacuum. $\Delta n = n_o - n_e$ is the difference between the indexes of refraction of ordinary light (n_o) and extraordinary light (n_e), which can be treated as a constant of 0.01 for the small frequency distribution. The amplitude decay channel in the dotted pane M' is simulated by a set of glass slabs (GS) tilted near Brewster's angle (about 57°) [14]. After the photon passing through the slabs, the vertical part has some probability to reflect and the horizontal part transmits completely. Therefore, the corresponding quantum map [15] can be written as $|H\rangle_S|0\rangle_E \rightarrow |H\rangle_S|0\rangle_E$ and $|V\rangle_S|0\rangle_E \rightarrow \sqrt{1-\varepsilon}|V\rangle_S|0\rangle_E + \sqrt{\varepsilon}|H\rangle_S|1\rangle_E$, where $|0\rangle_E$ and $|1\rangle_E$ represent the propagation paths of the photon and ε represents the total reflectivity of the glass slabs (the polarization of the reflected part is changed into $|H\rangle$).

The half wave plate (HWP1) with optic axis set at 22.5° operates as a Hadamard gate and $Q1$ with optic axis set at horizontal can induce relative phase in the basis H/V. They are inserted into mode a depending on different cases to prepare different initial states.

The density matrices of the final states are reconstructed by the tomography process [2]. Experimentally, quarter wave plates (QWP), half wave plates (HWP), and polarization beam splitters (PBS) in both arms are used to set the standard 16 polarization analysis measurement bases [2]. Both photons are detected by silicon avalanche photodiodes $D1$ and $D2$ to give coincident counts. Interference filters (IF) with a full width at half maximum (FWHM) of 3 nm in front of detectors are used to reduce the background and define the bandwidth of the photons.

We first demonstrate the entanglement dynamics of different pure input states in the phase damping channel in Fig. 2. The x axis represents total thickness of $Q2$ which is given by its retardation. Figure 2(a) shows the case with $\alpha^2 = \frac{1}{2}$ (the maximally entangled state $|\phi^+\rangle$), which is the trivial result of Eq. (2). The concurrence of the initial state is about 0.953. It is shown that the experimental results of C_{LP} and C_{RP} agree very well, which are represented by red dots and blue squares, respectively. Two other cases with $\alpha^2 = \frac{1}{5}$ and $\frac{1}{10}$ are illustrated in Figs. 2(b) and 2(c), where we find that Eq. (2) holds too. Solid lines and dashed lines

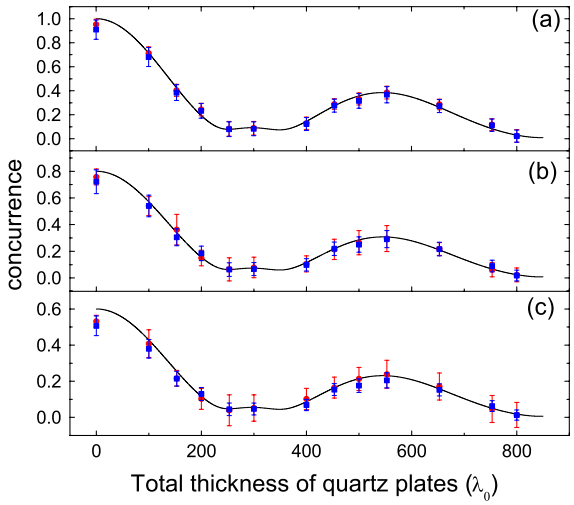

FIG. 2 (color online). Experimental results of different pure initial states in the phase damping channel. (a) $\alpha^2 = \frac{1}{2}$, (b) $\alpha^2 = \frac{1}{5}$, (c) $\alpha^2 = \frac{1}{10}$. Red dots and blue squares represent C_{LP} and C_{RP}, respectively. Solid lines and dashed lines representing the theoretical predictions of C_{LP} and C_{RP} completely overlap (as a result, only the solid lines can be seen). $\lambda_0 = 780$ nm.

representing the theoretical predictions of C_{LP} and C_{RP} completely overlap in Fig. 2, which are calculated from Eq. (1). In such a dephasing channel, the decoherence parameter is given by $\kappa_b = \int f(\omega_b)\exp(i\delta_b)d\omega_b$, where $f(\omega_b)$ denotes the amplitude corresponding to the frequency ω_b of the photon in mode b with $\int f(\omega_b)d\omega_b = 1$. For the theoretical fittings, the frequency distribution in mode a is treated as the Gaussian wave function with central wavelength 780 nm, which is defined by the 3 nm interference filter. Discrete frequency distributions filtered by the FP cavity in mode b are treated as three Gaussian wave packets centered at 778.853, 780.160, and 781.459 nm with relative probabilities of 0.37, 0.44, and 0.19, respectively [13]. Their spectrum widths are identically fitted to 0.85 nm [13]. During the evolution, due to the discrete frequency distribution in the phase damping channel, the overall relative phase refocuses and the dynamics of entanglement exhibits the property of collapse and revival [13]. We can find from Fig. 2 that experimental results are consistent with theoretical predictions. Error bars are mainly due to the counting statistics and the uncertainties in aligning the wave plates [2].

When it comes to the case with mixed input states, C_{RM} gives the upper bound of the evolved entanglement according to the inequality (3). Figure 3(a) shows the case with the mixed input state prepared by only inserting $Q1 = 117\lambda_0$ into mode a to dephase the maximally entangled state $|\phi^+\rangle$. Because of the symmetry of the initial mixed state, i.e., $\rho_0 = (\$' \otimes \mathbb{1})|\phi^+\rangle\langle\phi^+| = (\mathbb{1} \otimes \$')|\phi^+\rangle\langle\phi^+|$, it satisfies the condition under which the equality holds in (3) [9]. Red dots and blue squares represent the experimental results of Γ_{LM} and Γ_{RM} [the quantity Γ is defined in Eq. (1) and the meanings of the subscripts are the same as that of concurrence C]. Solid lines and dashed lines are the corresponding theoretical predictions. In this case, $C = \Gamma$ and it is shown that experimental results agree well with theoretical predictions $C_{\mathrm{LM}} = C_{\mathrm{RM}}$. We further demonstrate the case in which the HWP1 is used to transform $|\phi^+\rangle$ into $1/2(|HH\rangle_{a,b} + |VH\rangle_{a,b} + |HV\rangle_{a,b} - |VV\rangle_{a,b})$ and $Q1 = 117\lambda_0$ is adopted to introduce the dephasing effect in mode a. In this case, the initial mixed state does not have the symmetry any more. Figure 3(b) shows our experimental results, where the phenomenon of entanglement sudden death occurs [13,16]. At the area of the quantity $\Gamma_{\mathrm{LM}} < 0$ (the theoretical prediction is represented by dotted lines), the concurrence (C_{LM}) is set to 0 according to Eq. (1) [8]. It can be seen that C_{LM} (red dots) are less than C_{RM} (blue squares) during the evolution, which is consistent with the theoretical prediction. From Fig. 3(b), we can see that Γ_{LM} and C_{RM} exhibit essentially the same functional dependence on the thickness of quartz plates. Although the experimental data of C_{RM} are close to zero, given the error bars, in the thickness interval from about $200\lambda_0$ to $400\lambda_0$, the relationship of $C_{\mathrm{LM}} < C_{\mathrm{RM}}$ still holds ($C_{\mathrm{LM}} = 0$ at this interval). As a result, C_{RM} actually provides the upper bound of the evolved entanglement.

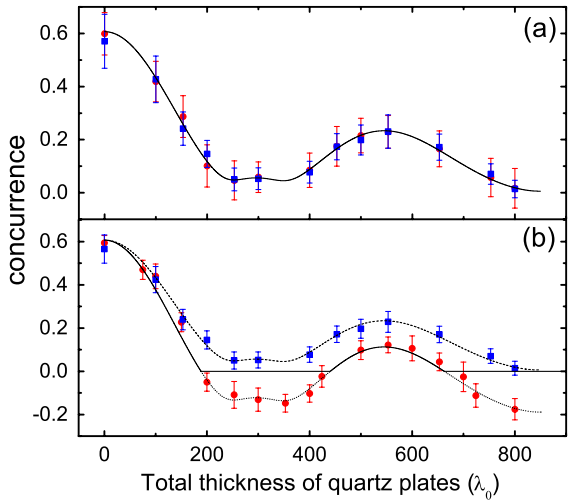

FIG. 3 (color online). Experimental results of different mixed input states in the phase damping channel. (a) The case with inserting only $Q1 = 117\lambda_0$ into mode a. (b) The case with inserting both the HWP1 and $Q1 = 117\lambda_0$ into mode a. Red dots are the experimental results of Γ_{LM} and blue squares represent Γ_{RM} [the quantity Γ is defined in Eq. (1) and the meanings of the subscripts are the same as that of concurrence C]. Solid lines and dashed lines are the theoretical predictions of C_{LM} and C_{RM}, respectively [they completely overlap in the case of (a)]. At the area of $\Gamma_{\mathrm{LM}} < 0$ [in the case of (b)] where the theoretical prediction is represented by dotted lines, the concurrence (C_{LM}) is set to 0 according to Eq. (1).

Then, we consider the entanglement dynamics in the amplitude decay channel, where the FP cavity and quartz plates $Q2$ in the dotted pane M are replaced by a set of glass slabs titled near Brewster's angle in the dotted pane M'. By changing the number of the glass slabs, we can control the interaction time between the photon and the channel. In order to compensate for the transverse displacement of the transmitted photons, symmetrically arranged slabs are added or removed in pairs [14]. The reflectivity of each pair of slabs is about 0.46. In this case, the final state is the mixture of the transmitted and reflected parts.

Figure 4 shows the experimental results of different pure input states $|\chi\rangle$ in the amplitude decay channel. Figures 4(a)–4(c) correspond to the initial state with $\alpha^2 = \frac{1}{2}$, $\frac{1}{5}$, and $\frac{1}{10}$, respectively. We can see that the experimental results of C_{LP} (red dots) are equal to C_{RP} (blue squares). The theoretical predictions of C_{LP} (solid lines) and C_{RP} (dashed lines) are both given by $2\alpha\beta\sqrt{1-\varepsilon}$; therefore, they completely overlap. The deviations between the experimental results and the corresponding theoretical predictions come mainly from the disturbance of the preparation of the initial state and the absorption of the slabs.

Figure 5 shows the experimental results of different mixed input states in the amplitude decay channel. The

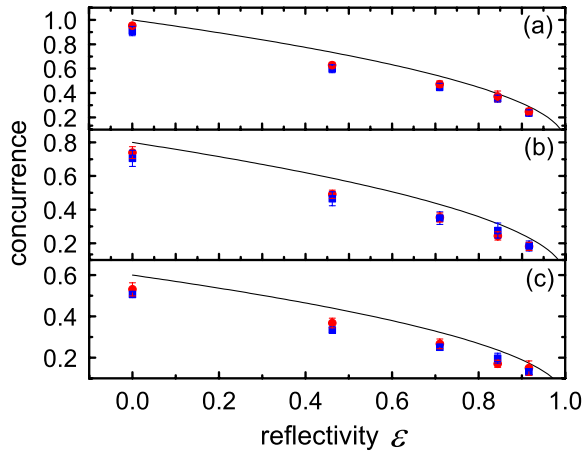

FIG. 4 (color online). Entanglement dynamics of different pure states in the amplitude decay channel. (a) $\alpha^2 = \frac{1}{2}$, (b) $\alpha^2 = \frac{1}{5}$, (c) $\alpha^2 = \frac{1}{10}$. Red dots and blue squares represent experimental results of C_{LP} and C_{RP}, respectively. The corresponding theoretical predictions of C_{LP} (solid lines) and C_{RP} (dashed lines) completely overlap and only the solid lines can be seen.

initial mixed state with the property of dephasing exchange symmetry in Fig. 5(a) is the same as that in Fig. 3(a), which is prepared by inserting only $Q1 = 117\lambda_0$ into mode a to dephase $|\phi^+\rangle$. As expected, we find that C_{LM} (red dots) are equal to C_{RM} (blue squares). The theoretical predictions of C_{LM} (solid lines) and C_{RM} (dashed lines) completely overlap and are consistent with the experimental results. In the other case where the initial mixed state without dephasing exchange symmetry is prepared by inserting both the HWP1 and $Q1 = 117\lambda_0$, we find that inequality (3) holds, as shown in Fig. 5(b). Experimental results agree with the corresponding theoretical prediction deduced from Eq. (1).

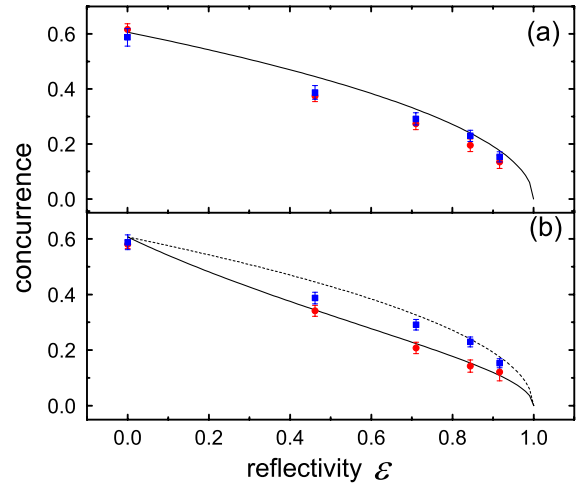

FIG. 5 (color online). Entanglement dynamics of different mixed input states in the amplitude decay channel. (a) The case with inserting only $Q1 = 117\lambda_0$ into mode a. (b) The case with inserting both the HWP1 and $Q1 = 117\lambda_0$ into mode a. Experimental results are represented by red dots (C_{LM}) and blue squares (C_{RM}). Solid lines and dashed lines are the corresponding theoretical fittings of C_{LM} and C_{RM} [they completely overlap in the case of (a)].

In conclusion, we have presented the general experimental result on open system entanglement dynamics and verified the factorization law [9]. Our experimental demonstration includes both the entanglement dynamics of pure and mixed initial two-photon states under the one-sided phase damping and amplitude decay channel, and we find very good agreement with the theoretical predictions. Our results provide a novel method to describe entanglement dynamics in noisy channels and would play important roles on the construction of complex quantum networks [17].

We thank Y. X. Gong for his notification. This work was supported by National Fundamental Research Program, the Innovation funds from Chinese Academy of Sciences, National Natural Science Foundation of China (Grant No. 60121503, 10874162), and Chinese Academy of Sciences International Partnership Project.

*cfli@ustc.edu.cn
†xbz@ustc.edu.cn

[1] M. A. Nielsen and I. L. Chuang, *Quantum Computation and Quantum Information* (Cambridge University Press, Cambridge, England, 2000).
[2] D. F. V. James, P. G. Kwiat, W. J. Munro, and A. G. White, Phys. Rev. A **64**, 052312 (2001).
[3] F. Mintert, A. R. R. Carvalho, M. Kuś, and A. Buchleitner, Phys. Rep. **415**, 207 (2005).
[4] K. Życzkowski, P. Horodecki, M. Horodecki, and R. Horodecki, Phys. Rev. A **65**, 012101 (2001).
[5] A. R. R. Carvalho, F. Mintert, and A. Buchleitner, Phys. Rev. Lett. **93**, 230501 (2004).
[6] W. Dür and H.-J. Briegel, Phys. Rev. Lett. **92**, 180403 (2004).
[7] A. R. R. Carvalho, M. Busse, O. Brodier, C. Viviescas, and A. Buchleitner, Phys. Rev. Lett. **98**, 190501 (2007).
[8] W. K. Wootters, Phys. Rev. Lett. **80**, 2245 (1998).
[9] T. Konrad, F. de Melo, M. Tiersch, C. Kasztelan, A. Aragão, and A. Buchleitner, Nature Phys. **4**, 99 (2008).
[10] O. J. Farías, C. L. Latune, S. P. Walborn, L. Davidovich, and P. H. S. Ribeiro, Science **324**, 1414 (2009).
[11] P. G. Kwiat, E. Waks, A. G. White, I. Appelbaum, and P. H. Eberhard, Phys. Rev. A **60**, R773 (1999).
[12] J.-S. Xu, C.-F. Li, and G.-C. Guo, Phys. Rev. A **74**, 052311 (2006).
[13] J.-S. Xu, *et al.*, arXiv:0903.5233.
[14] P. G. Kwiat, S. Barraza-Lopez, A. Stefanov, and N. Gisin, Nature (London) **409**, 1014 (2001).
[15] J. Preskill, http://www.theory.caltech.edu/people/preskill/ph229/notes/chap3.pdf).
[16] T. Yu and J. H. Eberly, Science **323**, 598 (2009).
[17] H. J. Kimble, Nature (London) **453**, 1023 (2008).